

Figure 1. Global map of all samples analyzed in this study. The number in each marker corresponds to the sample group number in Tables 1 and 2.

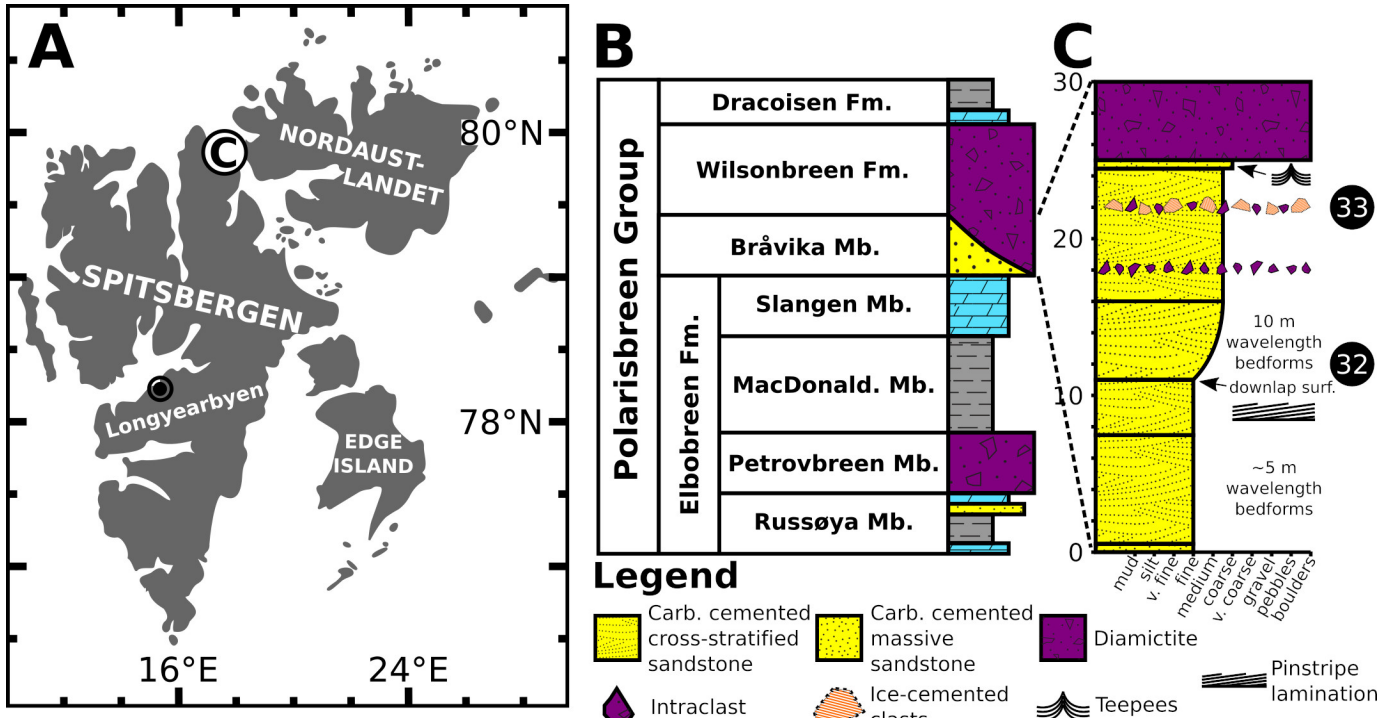


Figure 2. Geologic context and stratigraphy of the Cryogenian Bråvika Member in Svalbard. A) Map of the Svalbard archipelago. The white circle on the map indicates the location of Buldrevågen and the stratigraphic column in C. B) Generalized stratigraphic nomenclature for the Cryogenian Polarisbreen Group in Svalbard after Halverson et al. (2018). As shown here, the Bråvika Member is assigned to neither the Wilsonbreen nor the Elbobreen formations, as its assignment is a key question explored in this study. The Petrovbrean Member is correlated with the Sturtian pan-glaciation and the Wilsonbreen Formation is correlated with the Marinoan pan-glaciation (Hoffman et al. 2012). The MacDonaldryggen and Slangen members are correlated with the Cryogenian interglacial (Fairchild et al. 2016). C) Stratigraphic column of the Bråvika Member at Buldrevågen. The black circles indicate where samples 32 (J1701-156) and 33 (J1701-166) were collected for microtextural analysis.

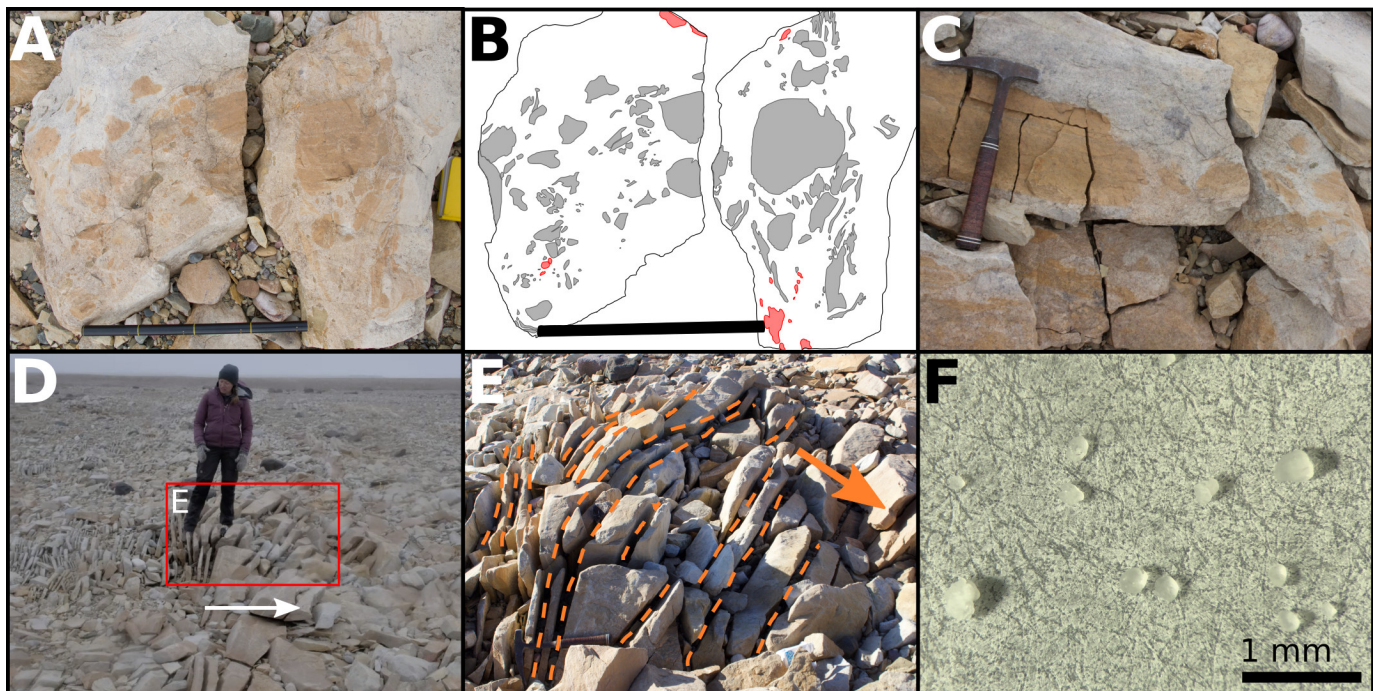


Figure 3. Field photos of the Bråvika Member in Buldrevågen, Svalbard. A) Photograph of sand intraclasts with diffuse boundaries and light green intraclasts at 22 m in Buldrevågen (© K.D. Bergmann 2017). Bar is 40 cm long. B) Line drawing of photograph in A at the same scale; gray clasts are the sand intraclasts with diffuse boundaries and red clasts are the light green intraclasts. C) Close-up of sand intraclasts with diffuse edges (© K.D. Bergmann 2017). D) Photograph of frost-shattered trough crossbedding at 12 m in Buldrevågen, where the fracture planes are bedding surfaces (© A.B. Jost 2017). Arrow points upsection. The box highlights the location of E) close-up of trough crossbedding (© K.D. Bergmann 2017). The dashed lines trace bedding surfaces and the arrow points upsection. F) Photomicrograph of frosted grains from the Bråvika Member in Buldrevågen after disaggregation.

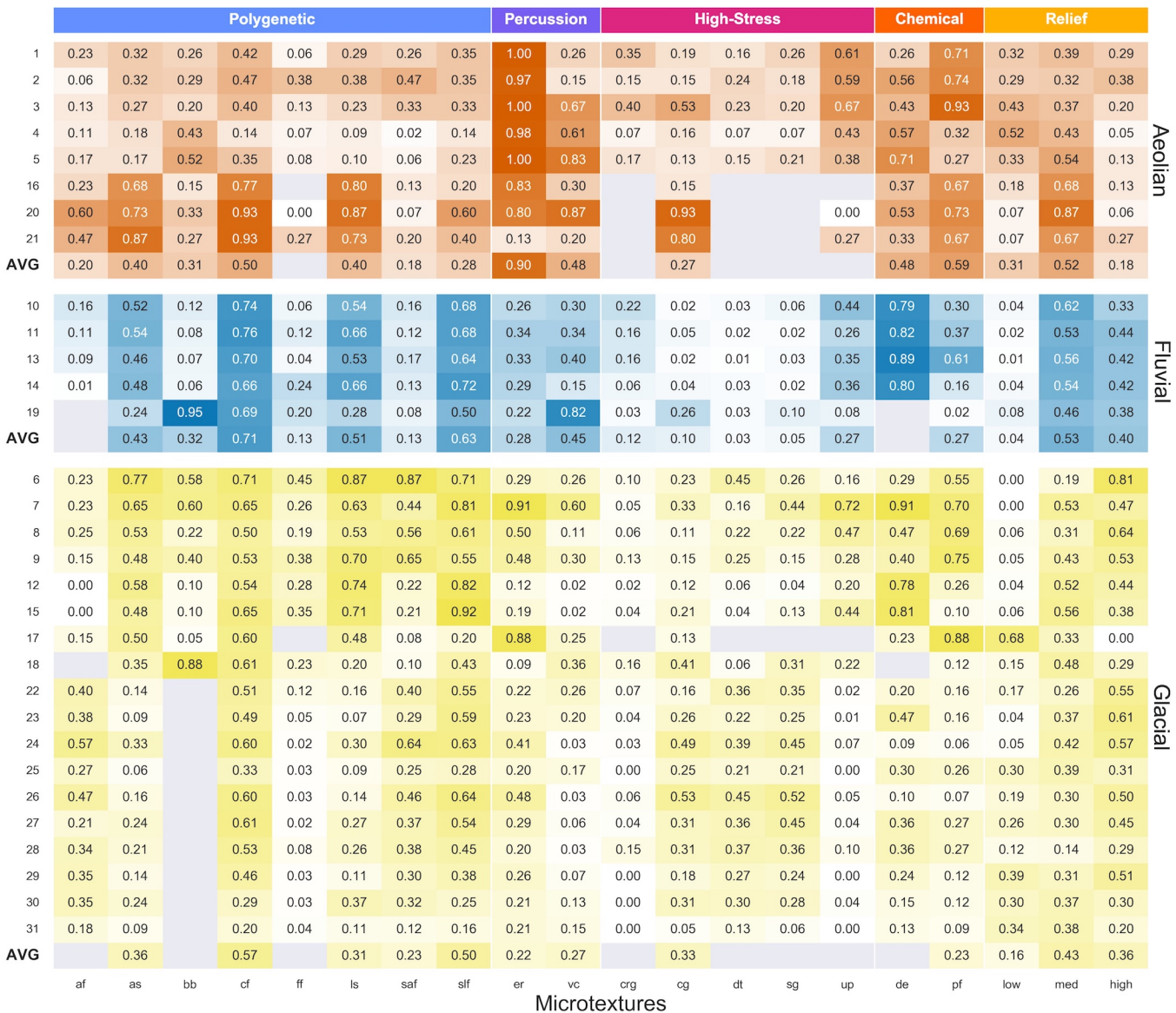


Figure 4. Heatmap of the microtextural probabilities of occurrence from 0 to 1 for each modern sample group used in the analysis. Samples are binned into aeolian, fluvial, and glacial transport modes. Refer to Table 1 for sample group numbers and descriptions. Data are averaged for sample groups that contain more than one sample ( $S > 1$ ). Refer to Table 3A and B for microtextural abbreviations. The average of each transport mode for the modern samples (AVG) is at the bottom of each bin. All averages were calculated using Equation 1. Microtextures that were not analyzed within a study are grayed out.

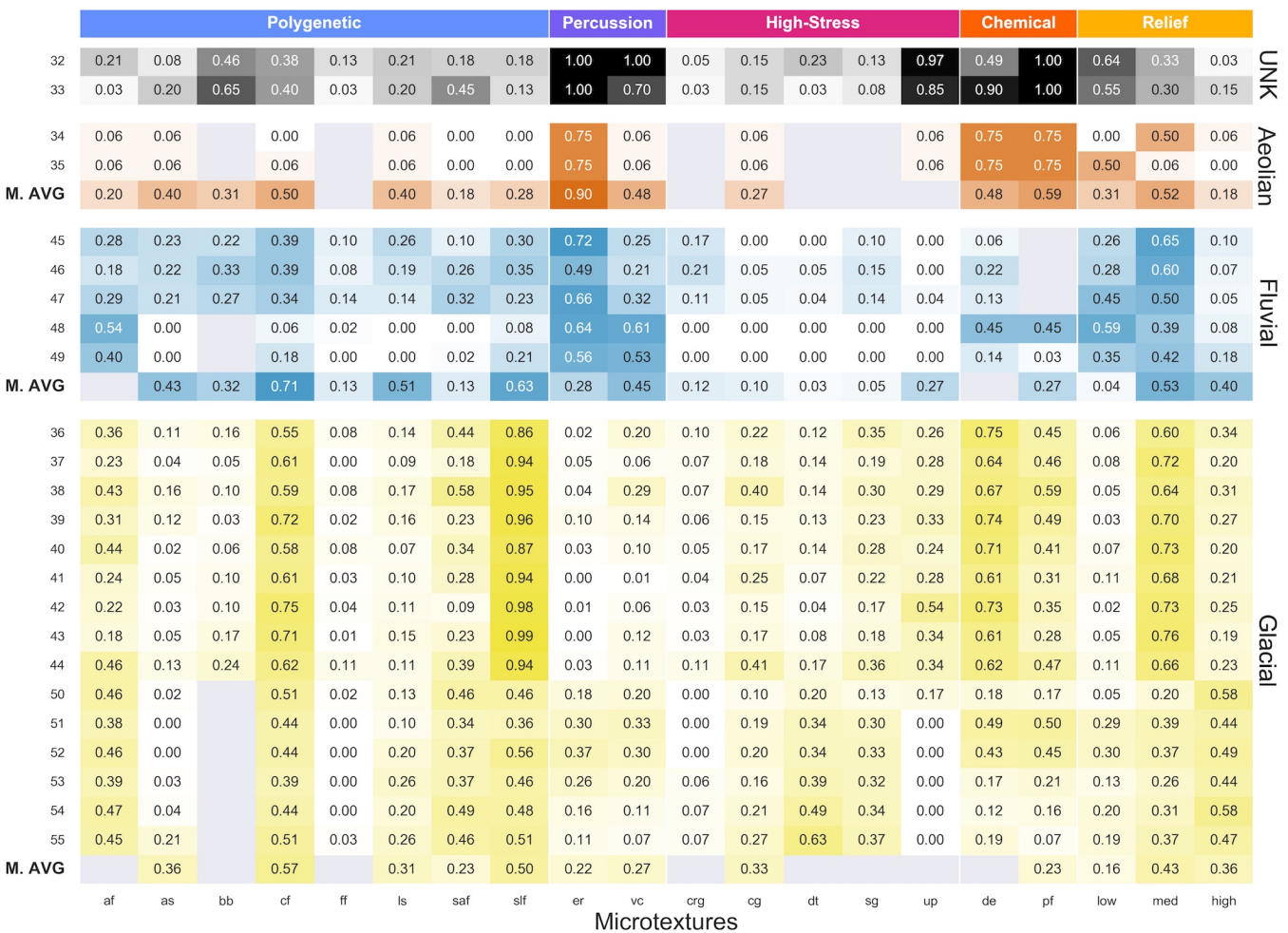


Figure 5. Heatmap of the microtextural probabilities of occurrence from 0 to 1 for each ancient sample group used in the analysis. Samples are binned into “unknown” (UNK; Bråvika Member), aeolian, fluvial, and glacial transport modes. Refer to Table 1 for sample group numbers and descriptions. Data are averaged for sample groups that contain more than one sample ( $S > 1$ ). Refer to Table 3A and B for microtextural abbreviations. The average of each transport mode for the modern samples (M. AVG) from Figure 4 is at the bottom of each bin. All averages were calculated using Equation 1. Microtextures that were not analyzed within a study are grayed out.

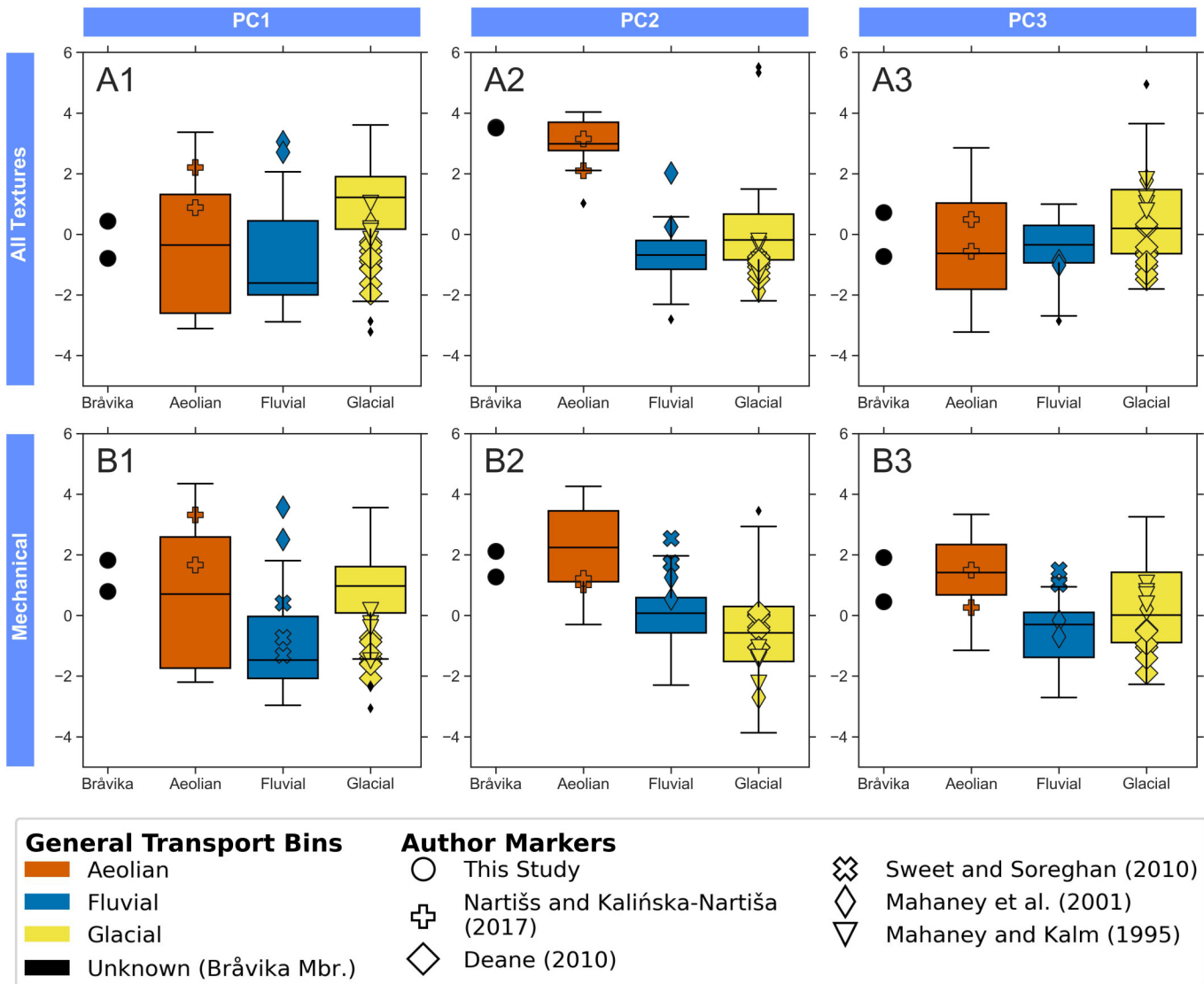


Figure 6. Boxplots of the modern aeolian, fluvial, and glacial samples (box and whiskers) in the all-textures PCA ordination (row A) and the mechanical ordination (row B). Each column represents a principal component axis in each ordination: PC1 (column 1), PC2 (column 2), and PC3 (column 3). The small black diamonds represent modern outliers for each transport mode. The ancient samples are plotted as individual points over the boxplots.

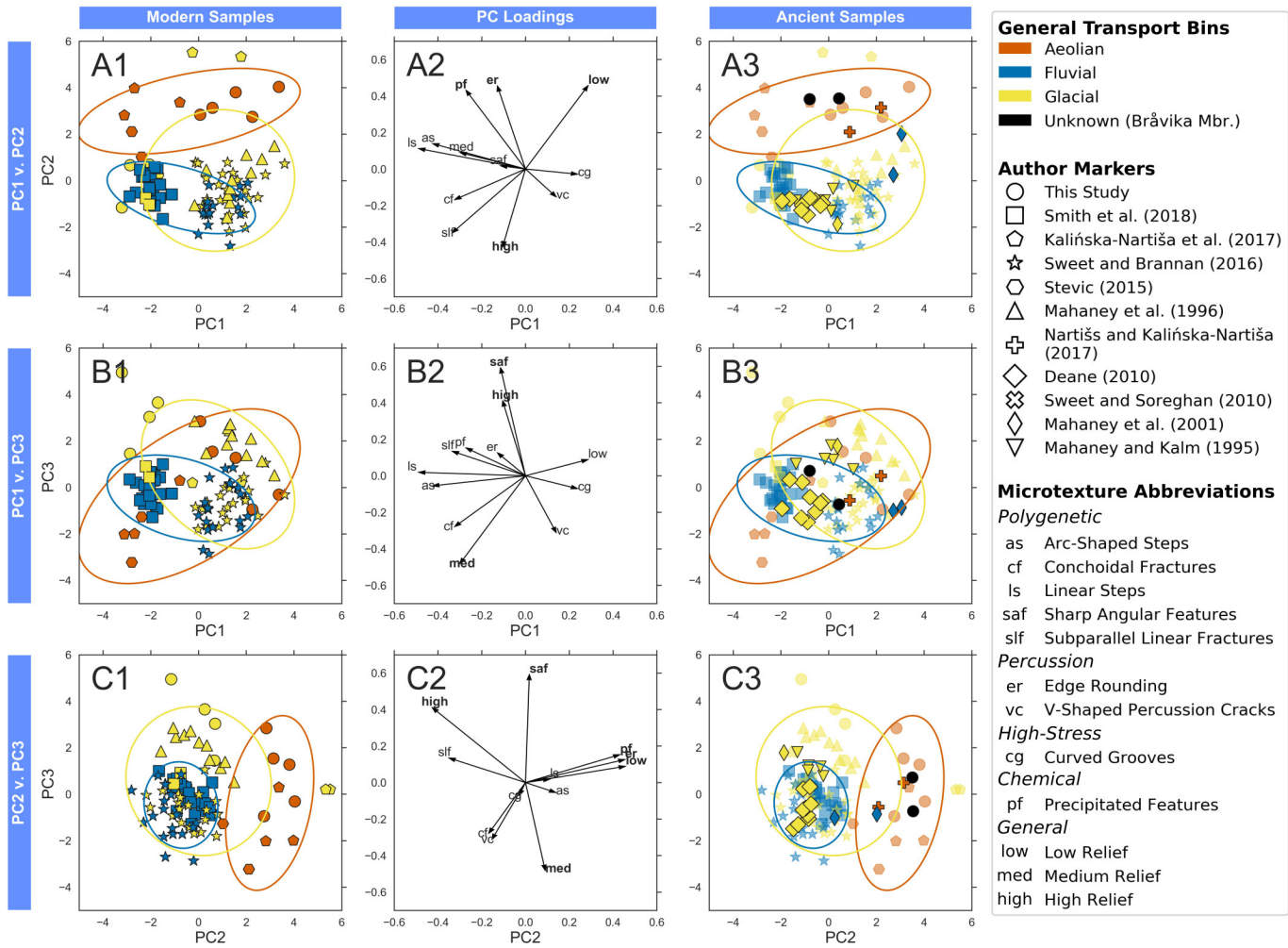


Figure 7. All-textures PCA ordination using all 12 microtextures analyzed by all authors. Each row is a biplot in A) PC1-PC2 space; B) PC1-PC3 space; and C) PC2-PC3 space. Column 1 plots the modern sample data within each space (this study through Mahaney et al. 1996), Column 2 plots the microtextural loadings, and Column 3 plots the ancient sample data (this study, Nartišs and Kalińska-Nartiša 2017 through Mahaney and Kalm 1995) over the existing modern reference frame. Refer to Table 5 for the loadings in Column 2. Microtextures with significant loadings in Column 2 are in bold. The ellipses are 95% confidence intervals of each modern transport mode that are centered at the mean of the transport mode in each coordinate space. The ellipses are calculated using the methods of Schelp (2019).

#### General Transport Bins

- Aeolian
- Fluvial
- Glacial
- Unknown (Bråvika Mbr.)

#### Author Markers

- This Study
- Smith et al. (2018)
- △ Kalińska-Nartiša et al. (2017)
- ☆ Sweet and Brannan (2016)
- Stevic (2015)
- △ Mahaney et al. (1996)
- + Nartišs and Kalińska-Nartiša (2017)
- ◊ Deane (2010)
- ⊗ Sweet and Soreghan (2010)
- ◇ Mahaney et al. (2001)
- ▽ Mahaney and Kalm (1995)

#### Microtexture Abbreviations

##### Polygenetic

- as Arc-Shaped Steps
- cf Conchoidal Fractures
- ls Linear Steps
- saf Sharp Angular Features
- slf Subparallel Linear Fractures

##### Percussion

- er Edge Rounding
- vc V-Shaped Percussion Cracks

##### High-Stress

- cg Curved Grooves

##### Chemical

- pf Precipitated Features

##### General

- low Low Relief

- med Medium Relief

- high High Relief

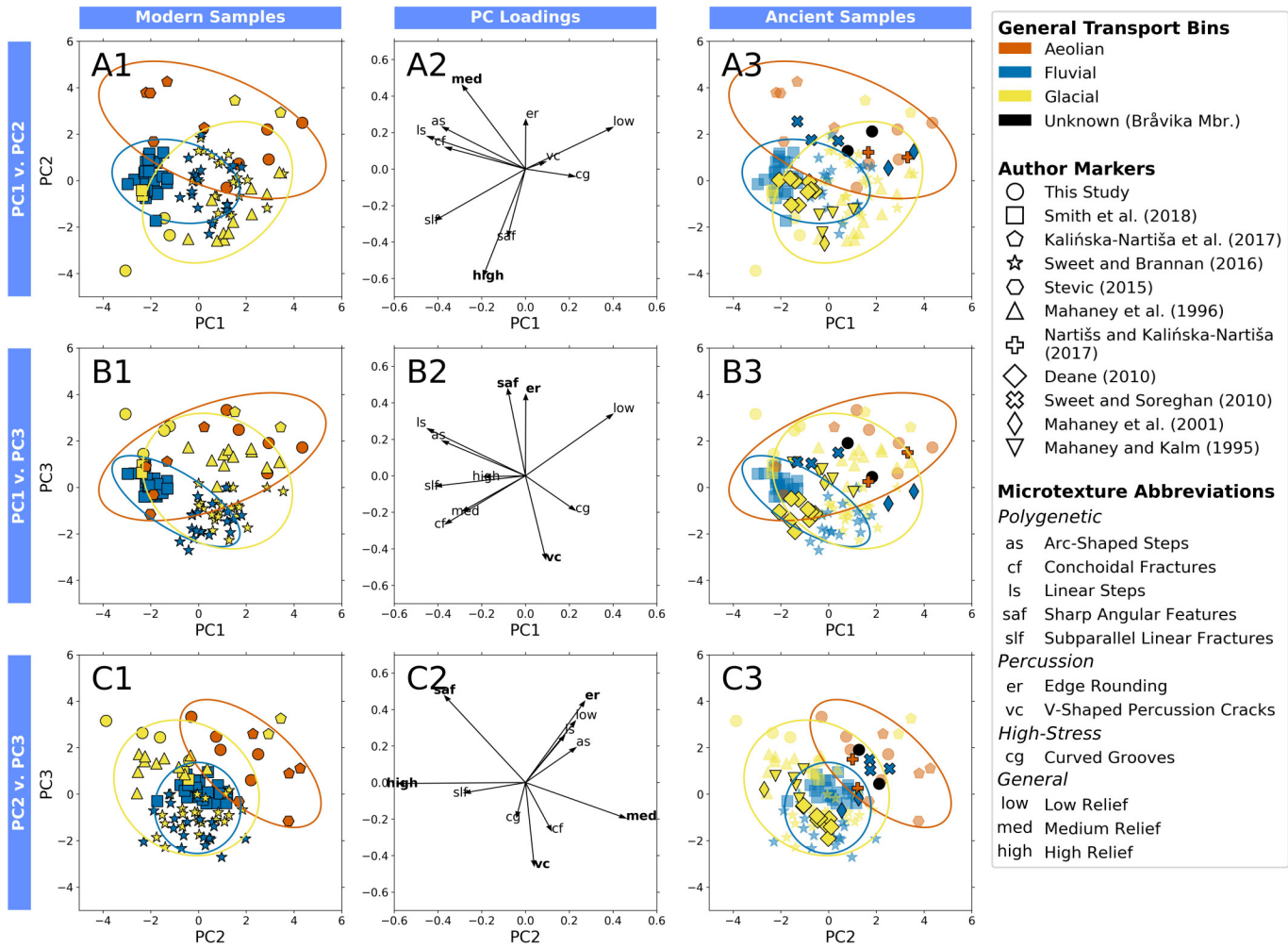


Figure 8. Mechanical PCA ordination using all 11 mechanical microtextures analyzed by all authors. These plots are in the same format as shown in Figure 7: each row is a biplot in A) PC1-PC2 space; B) PC1-PC3 space; and C) PC2-PC3 space. Column 1 plots the modern sample data within each space (this study through Mahaney et al. 1996), Column 2 plots the microtextural loadings, and Column 3 plots the ancient sample data (this study, Nartišs and Kalińska-Nartiša 2017 through Mahaney and Kalm 1995) over the existing modern reference frame. Refer to Table 6 for the loadings in Column 2. Microtextures with significant loadings in Column 2 are in bold. The ellipses are 95% confidence intervals of each modern transport mode that are centered at the mean of the transport mode in each coordinate space. The ellipses are calculated using the methods of Schelp (2019).

Table 1. List of the samples from modern depositional environments considered in this study. Each group of samples is assigned a number for later reference in Figures 1 and 4 (Column #). Column S indicates the number of samples in each sample group, and column N indicates the number of quartz grains in each sample group.

Study	#	Sample Location	Transport	S	N	GPS Point
This Study	1	Lake Fryxell, McMurdo Dry Valleys, Antarctica	Aeolian	1	31	77°36'48"S, 163°06'40"E
	2	Lake Joyce, McMurdo Dry Valleys, Antarctica	Aeolian	1	34	77°43'11"S, 161°36'25"E
	3	Lake Vanda, McMurdo Dry Valleys, Antarctica	Aeolian	1	30	77°31'38"S, 161°36'24"E
	4	Algodones Dunes, California, U.S.	Aeolian	1	44	33°08'57"N, 115°18'48"W
	5	Waynoka Dunes, Oklahoma, U.S.	Aeolian	1	48	36°33'35"N, 98°53'56"W
	6	Llewellyn Glacier, B.C. (JIF19-C26-01)	Glacial	1	31	59°00'49"N, 134°07'15"W
	7	Llewellyn Glacier, B.C. (JIF19-C26-02)	Glacial	1	39	59°00'48"N, 134°07'13"W
	8	Llewellyn Glacier, B.C. (JIF19-C26-03)	Glacial	1	36	59°00'48"N, 134°07'13"W
	9	Llewellyn Glacier, B.C. (JIF19-C26-04)	Glacial	1	40	59°00'50"N, 134°07'14"W
Smith et al. (2018)	10	Anza-Borrego Desert, California, U.S.	Fluvial	5	250	32°54'00"N, 116°16'00"W
	11	Auster and Storelvå Rivers, Norway	Fluvial	7	346	61°32'00"N, 06°57'00"E
	12	Austerdal Glacier Moraine, Norway	Glacial	1	50	61°32'00"N, 06°57'00"E
	13	Rio Guayanés, Puerto Rico	Fluvial	6	297	18°03'00"N, 65°54'00"W
	14	Rio Parón, Peru	Fluvial	5	250	09°00'00"S, 77°42'00"W
Kalińska-Nartışa et al. (2017)	15	Moraine Proximal to Lake Parón, Peru	Glacial	1	48	09°00'00"S, 77°42'00"W
	16	Russell Glacier, Greenland (CE1, CE2, CE8)	Aeolian	3	60	67°05'00"N, 50°20'00"W
	17	Russell Glacier, Greenland (CE12, CE13)	Glacial	2	40	67°07'00"N, 50°05'00"W
Sweet and Brannan (2016)	18	Chitina Glacier Moraine to 12 km Past Tana River Confluence, Alaska, U.S. (CR-1 to CR-23)	Glacial	22	626	61°05'44"N, 142°11'03"W
	19	12 km Past Tana River Confluence to the Copper River, Alaska, U.S. (CR-24 to CR-41)	Fluvial	18	450	61°21'42"N, 143°46'34"W
Stevic (2015)	20	Coastal Sand Dune, Vittskövle, Sweden	Aeolian	1	15	55°51'56"N, 14°10'02"E
	21	Inland Sand Dune, Brattforsheden, Sweden	Aeolian	1	15	59°36'26"N, 13°53'03"E
Mahaney et al. (1996)	22	Lichen Valley, Vestfold Hills, Antarctica (Site A)	Glacial	1	25	68°28'53"S, 78°10'24"E
	23	Ackerman Ridge, Scott Glacier area, Antarctica (Sites B – C)	Glacial	1	25	85°45'00"S, 153°00'00"W
	24	Southern Inexpressible Island, Antarctica (Site D)	Glacial	1	25	74°54'00"S, 163°39'00"E
	25	Taylor Glacier, McMurdo Dry Valleys, Antarctica (Site E)	Glacial	1	25	77°44'00"S, 162°10'00"E
	26	Hatherton Glacier, Antarctica (Site F)	Glacial	1	25	79°55'00"S, 157°35'00"E
	27	Roberts Massif, Antarctica (Sites G – H)	Glacial	2	50	85°32'00"S, 177°05'00"W
	28	Barwick Valley, Antarctica (Site I)	Glacial	1	25	77°23'24"S, 161°02'18"E
	29	Cambridge Glacier, Antarctica (Site J)	Glacial	1	25	76°57'00"S, 160°31'00"E
	30	Southern Inexpressible Island, Antarctica (Site D)	Glacial	1	25	75°38'00"S, 161°05'00"E
	31	Luther Peak Basin, Edisto Inlet, Antarctica (Site L)	Glacial	1	25	72°22'00"S, 169°50'00"E

Table 2. List of the samples from ancient depositional environments considered in this study. Each group of samples is assigned a number for reference in Figures 1, 2, and 5 (Column #). Column S indicates the number of samples in each sample group, and column N indicates the number of quartz grains in each sample group.

Study	#	Sample	Transport	S	N	GPS Point	Geologic Period
This Study	32	Bråvika Mbr.– Buldrevågen (J1701-156)	Unknown	1	39	78°09'29"N, 17°31'20"E	Cryogenian
	33	Bråvika Mbr.– Buldrevågen (J1701-166)	Unknown	1	40	78°09'29"N, 17°31'20"E	
Nartišs and Kalińska-Nartiša (2017)	34	Middle Gauja Lowland, Latvia (Mielupīte 1.3)	Aeolian	1	16	57°30'00"N, 26°00'00"E	Pleistocene
	35	Middle Gauja Lowland, Latvia (Mielupīte 1.7)	Aeolian	1	18	57°30'00"N, 26°00'00"E	
Deane (2010)	36	Till, Costa Rica (Sample 2)	Glacial	1	300	09°29'35"N, 83°29'07"W	
	37	Till, Costa Rica (Sample 3)	Glacial	1	100	09°29'35"N, 83°29'07"W	
	38	Till, Costa Rica (Sample 4)	Glacial	1	100	09°29'35"N, 83°29'07"W	
	39	Till, Costa Rica (Sample 5)	Glacial	1	100	09°29'35"N, 83°29'07"W	
	40	Till, Costa Rica (Sample 8)	Glacial	1	100	09°29'35"N, 83°29'07"W	Pleistocene
	41	Till, Dominican Republic (Sample 10)	Glacial	1	100	19°02'01"N, 71°04'22"W	
	42	Till, Dominican Republic (Sample 11)	Glacial	1	100	19°01'60"N, 71°04'26"W	
	43	Till, Dominican Republic (Sample 17)	Glacial	1	100	19°02'07"N, 71°04'38"W	
	44	Till, Dominican Republic (Sample 18)	Glacial	1	100	19°01'39"N, 71°02'30"W	
Sweet and Soreghan (2010)	45	Upper Fountain Fm., Colorado, U.S.	Fluvial	3	47	38°51'24"N, 104°54'36"W	Pennsylvanian-Lower Permian
	46	Middle Fountain Fm., Colorado, U.S.	Fluvial	8	125	38°51'24"N, 104°54'36"W	
	47	Lower Fountain Fm., Colorado, U.S.	Fluvial	4	62	38°51'24"N, 104°54'36"W	
Mahaney et al. (2001)	48	Arküla Stage Sandstone, Estonia	Fluvial	21	420	58°15'00"N, 26°30'00"E	Middle Devonian
	49	Glaciofluvial Sand, Estonia	Fluvial	3	60	58°15'00"N, 26°30'00"E	Pleistocene
	50	Till, Estonia	Glacial	29	580	58°15'00"N, 26°30'00"E	
Mahaney and Kalm (1995)	51	Latvia Till, Estonia	Glacial	5	100	58°13'28"N, 26°25'16"E	
	52	Varduva Till, Estonia	Glacial	5	100	58°13'28"N, 26°25'16"E	
	53	Upper Ugandi Till, Estonia	Glacial	5	100	58°13'28"N, 26°25'16"E	Pleistocene
	54	Lower Ugandi Till, Estonia	Glacial	5	100	58°13'28"N, 26°25'16"E	
	55	Upper Dainava Till, Estonia	Glacial	3	60	58°13'28"N, 26°25'16"E	

Table 3A. Photos and description of microtextures used in this study. Scale bars are 100 µm unless otherwise noted.

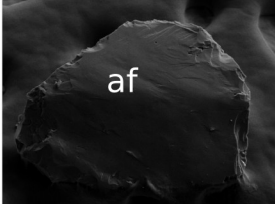
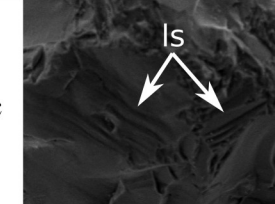
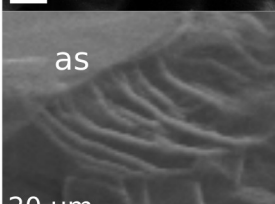
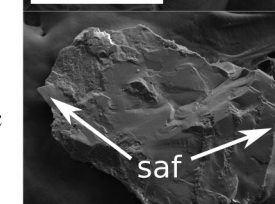
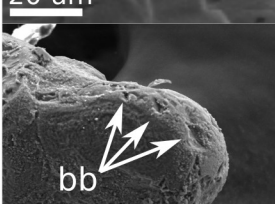
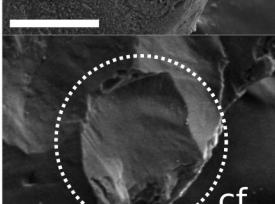
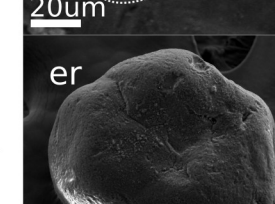
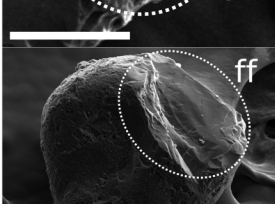
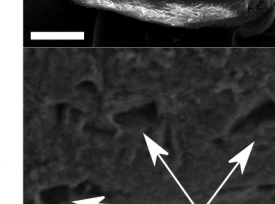
Microtexture	Abbr.	Description	Formation Process	Example Photo	Microtexture	Abbr.	Description	Formation Process	Example Photo
Abrasion Features	af	Rubbed or worn surface	Polygenetic		Linear Steps	ls	Widely spaced linear features, typically >5 µm apart	Polygenetic	
Arc-Shaped Steps	as	Deep tears or breaks caused by impact; Several microns deep and typically spaced > 5 µm apart	Polygenetic		Sharp Angular Features	saf	Distinct sharp edges on grain surface	Polygenetic	
Breakage Blocks	bb	Blocky void marking removal of material, typically along an edge	Polygenetic		Subparallel Linear Fractures	slf	Linear fractures, typically <5 µm spacing	Polygenetic	
Conchoidal Fractures	cf	Smooth, curved fracture	Polygenetic		Edge Rounding	er	Rounded edges on grains	Percussion	
Fracture Faces	ff	Smooth and clean fractures	Polygenetic		V-Shaped Percussion Cracks	vc	V-shaped fractures or indentations with typical sizes ranging from 1 µm to 30 µm	Percussion	

Table 3B. Photos and description of microtextures used in this study. Scale bars are 100  $\mu\text{m}$  unless otherwise noted.

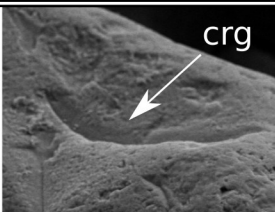
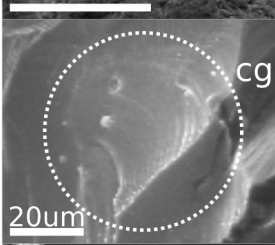
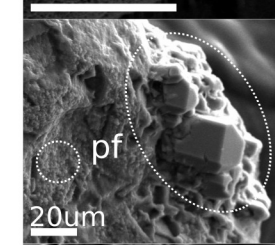
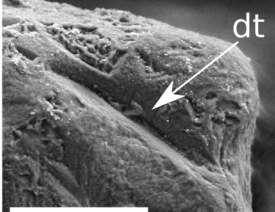
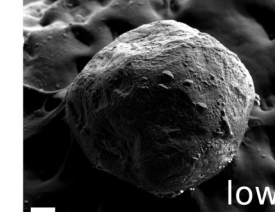
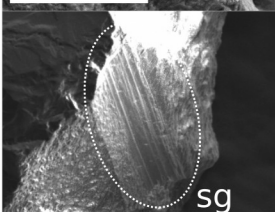
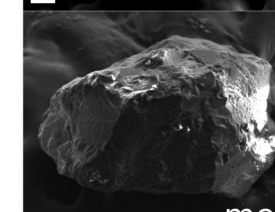
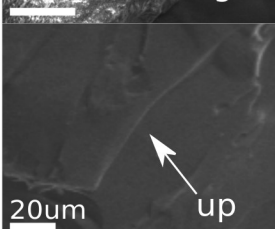
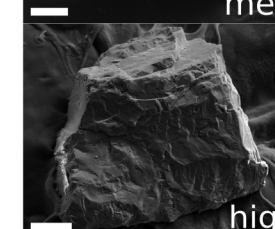
Microtexture	Abbr.	Description	Formation Process	Example Photo	Microtexture	Abbr.	Description	Formation Process	Example Photo
Crescentic Gouges	crg	Crescent-shaped gouges with convex and concave limbs that have depths $> 5 \mu\text{m}$	High-Stress		Dissolution Etching	de	Cavities from chemical dissolution; often crystallographically oriented	Chemical	
Curved Grooves	cg	Curved abrasion feature caused by sustained high-stress contact with another grain, $< 5 \mu\text{m}$ deep	High-Stress		Precipitation Features	pf	Coatings of amorphous silica precipitation	Chemical	
Deep Troughs	dt	Grooves $> 10 \mu\text{m}$ deep	High-Stress		Low Relief	low	Nearly smooth surface without topographic irregularities	Entire history of grain	
Straight Grooves	sg	Linear grooves $< 10 \mu\text{m}$ deep	High-Stress		Medium Relief	med	Semi-smooth surface with topographic irregularities	Entire history of grain	
Upturned Plates	up	Surfaces of impact where plates of variable size are partially torn from surface, typically $> 5 \mu\text{m}$	High-Stress		High Relief	high	Topographically irregular surface with pronounced swells and swales	Entire history of grain	

Table 4. Percentage variance of each principal component axis for each PCA ordination.

PCA Ordination	Axis	Individual	Cumulative
All Microtextures	PC1	27.01	27.01
	PC2	21.33	48.34
	PC3	17.43	65.77
Mechanical Microtextures	PC1	28.37	28.37
	PC2	20.04	48.41
	PC3	17.32	65.73

Table 5. Ranked loadings and squared loadings of microtextures from the all-textures PCA ordination (Figure 7). The microtextures in bold have squared loadings that are greater than the expected value of their associated principal component according to the broken-stick criterion (Frontier 1976; Jackson 1993; Legendre and Legendre 1998; Peres-Neto et al. 2003).

PC1			PC2			PC3		
Expected PC Value:	0.259	Microtexture	Expected PC Value:	0.175	Microtexture	Expected PC Value:	0.134	(Loading) <sup>2</sup>
Microtexture	Loading	(Loading) <sup>2</sup>	Microtexture	Loading	(Loading) <sup>2</sup>	Microtexture	Loading	(Loading) <sup>2</sup>
low	0.286	0.082	<b>low</b>	<b>0.457</b>	<b>0.209</b>	saf	<b>0.592</b>	<b>0.351</b>
cg	0.239	0.057	er	<b>0.455</b>	<b>0.207</b>	<b>high</b>	<b>0.411</b>	<b>0.169</b>
vc	0.141	0.020	<b>pf</b>	<b>0.432</b>	<b>0.186</b>	pf	0.153	0.023
high	-0.104	0.011	as	0.139	0.019	slf	0.135	0.018
saf	-0.114	0.013	ls	0.112	0.013	er	0.126	0.016
er	-0.128	0.017	med	0.090	0.008	low	0.089	0.008
pf	-0.272	0.074	saf	0.018	0.000	ls	0.019	0.000
med	-0.300	0.090	cg	-0.028	0.001	as	-0.055	0.003
cf	-0.324	0.105	vc	-0.153	0.023	cg	-0.071	0.005
slf	-0.335	0.112	cf	-0.168	0.028	cf	-0.279	0.078
as	-0.425	0.181	slf	-0.350	0.123	vc	-0.312	0.097
ls	-0.489	0.239	<b>high</b>	<b>-0.427</b>	<b>0.182</b>	<b>med</b>	<b>-0.482</b>	<b>0.232</b>

Table 6. Ranked loadings and squared loadings of microtextures from the mechanical PCA ordination (Figure 8). The microtextures in bold have squared loadings that are greater than the expected value of their associated principal component according to the broken-stick criterion (Frontier 1976; Jackson 1993; Legendre and Legendre 1998; Peres-Neto et al. 2003).

PC1			PC2			PC3		
Microtexture	Loading	(Loading) <sup>2</sup>	Microtexture	Loading	(Loading) <sup>2</sup>	Microtexture	Loading	(Loading) <sup>2</sup>
low	0.400	0.160	<b>med</b>	<b>0.460</b>	<b>0.211</b>	<b>saf</b>	<b>0.476</b>	<b>0.226</b>
cg	0.228	0.052	er	0.271	0.074	er	<b>0.446</b>	<b>0.199</b>
vc	0.093	0.009	as	0.231	0.053	low	0.338	0.114
er	0.001	0.000	low	0.229	0.052	ls	0.258	0.067
saf	-0.081	0.007	ls	0.180	0.032	as	0.192	0.037
high	-0.193	0.037	cf	0.119	0.014	high	-0.005	0.000
med	-0.289	0.084	vc	0.040	0.002	slf	-0.057	0.003
cf	-0.367	0.135	cg	-0.041	0.002	cg	-0.190	0.036
as	-0.381	0.145	slf	-0.282	0.079	med	-0.195	0.038
slf	-0.413	0.171	saf	-0.370	0.137	cf	-0.265	0.070
ls	-0.449	0.202	<b>high</b>	<b>-0.586</b>	<b>0.343</b>	<b>vc</b>	<b>-0.458</b>	<b>0.209</b>